Adsorption of chromium on activated carbon produced from agri-food waste

Abstract

The objective of this study is the adsorption of chromium on activated carbon produced from agri-food waste such as the shells of *Balanites aegyptiaca* (L.) Del. (Adoua), *Hyphaene thebaica* (L.) Mart. (Gorouba), *Zizyphus* mauritiana (L.) Lam. (Magaria) and Balanites aegyptiaca (L.) Del. cake by chemical activation with 25% orthophosphoric acid and 25% sulfuric acid. The mass yields of the ACs after pyrolysis, surface functions (Boehm method), pH at zero loading point (return dosage) and methylene blue (MB) adsorption capacities are determined. Next, the adsorption kinetics of chromium on the developed activated carbons (CAEs) and a commercial activated carbon (CA-C) are determined. The results show that the best yields are obtained with HT; 51.55% (H_3PO_4) and 40% (H_2SO_4). The surface functions are acidic in nature and range from 3.18 to 3.91 meq g^{-1}. The pH_{PCNs} vary from 1.3 to 5.24. The BM extraction rates vary from 83.3445 to 94.3777%. Elovich's correlation coefficients (R^2) are in the order of 0.96728 and 0.94642 for CA-BA-H_3PO_4 and CA-HT-H_3PO_4, respectively. The initial Cr adsorption rates "α" are 2.45343 $.10^{11}$ and 1.91005 $.10^{6}$ mg g^{-1} min^{-1} for CA-BA-H_3PO_4 and CA-HT-H_3PO_4, respectively. The material diffusivities D are 0.07643 and 0.13219 cm^2 min^{-1} for CA-BA-H_3PO_4 and CA-HT-H_3PO_4, respectively. The optimal adsorption pH values for chromium are 2 and 8 for CA-BA-H_3PO_4 and CA-HT-H_3PO_4, respectively. It should be noted that the yields of our three CAE samples exceed that of CAC (91.48%).

Keywords: Adsorption, Chromium, Activated Carbon, Kinetics, Agri-food Waste.

1. Introduction

Water is essential to life, but it is a resource that is very unevenly distributed around the world [1,2]. In addition, it is becoming increasingly polluted. Pollution that deteriorates water quality and the environment is caused by the discharge of mineral or organic substances that are more or less difficult to biodegrade, as well as other toxic substances [3,4]. The discharge of these effluents poses a major threat to humans and ecosystems. Africa accounts for approximately 9% of the planet's freshwater resources and 11% of the world's population. The

many water-related challenges facing sub-Saharan Africa are hampering its economic growth and threatening the livelihoods of its people [2]. Drinking water is a scarce commodity that must be protected from toxic substances that harm human health and ecosystems. Good quality water resources in sufficient quantities are necessary for economic development and the well-being of populations. In this regard, the leather and hide treatment techniques used in industrial and semi-industrial tanneries in Niger, which employ chromium salt-based formulations, as in many industrial tanneries around the world, have contributed significantly to water pollution [5-6]. The discharge of tannery wastewater most often generates effluents that do not comply with chromium discharge standards, set at 1 mg L^{-1} for discharge into sewers [7]. It is therefore essential to limit this pollution as much as possible by implementing a chromium removal technique adapted to our locality (Niger). There are various methods for removing chemicals (heavy metals, dyes, phenols, etc.) from effluents. Among these methods, adsorption is the most widely used technique due to its effectiveness, ease of implementation, and affordable investment cost [2,8-9].

This method requires the selection of an adsorbent with good characteristics (high adsorption capacity, availability, low cost, etc.) [10-12]. Microporous adsorbents such as activated carbons are widely used in the extraction of chemical species in aqueous or gaseous phases due to their excellent adsorption capacity [13-15]. In this topic, we will develop and characterize activated carbons from local lignocellulosic biomass, in particular the shells of the kernels of *Balanites aegyptiaca* (L.) Del. (Adoua), *Hyphaene thebaica* (L.) Mart. (Gorouba), *Zizyphus mauritiana* (L.) Lam. (Magaria), and *Balanites aegyptiaca* (L.) Del. cake through chemical activation with orthophosphoric acid and sulfuric acid. Next, the mass yields of the ACs after pyrolysis, surface functions, pH at zero charge point, and methylene blue (MB) adsorption capacities are determined on the one hand, and the kinetics and isotherms of chromium adsorption on the activated carbons produced are determined on the other.

2. Materials and methods

2.1. Synthesis of activated carbons

After conditioning the raw materials, the activated carbons are produced in three stages [5,15] :

- ✓ impregnation of the biomass in solutions of the activating agent;
- ✓ pyrolysis of the impregnated biomass;

- ✓ purification of the product obtained.

In this work, two activating agents are used, namely orthophosphoric acid (H_3PO_4) and sulfuric acid (H_2SO_4).

The activated carbon samples synthesized at the end of this optimization process are used to determine the mass yields after pyrolysis, the iodine (I_2) adsorption capacities, and the methylene blue (MB) adsorption capacities.

2.1.1. Activation of the biomass sample

In 250 mL beakers, 16 g of the pretreated raw material and 100 mL of the activating agent solution (H_3PO_4 and H_2SO_4) are mixed together. The mixture obtained is stirred for 15 hours on a magnetic stirrer at atmospheric pressure and room temperature. The sample is then filtered on ashless filter paper using a Büchner funnel, washed with distilled water, and dried in an oven at 105°C for 24 hours.

2.1.2. Pyrolysis of impregnated biomass samples

The dry sample obtained after impregnation was placed in a programmable high-temperature muffle furnace. The furnace temperature was gradually increased to the pyrolysis temperature (450°C) at a heating rate of 2.5°C min^{-1}, with an isothermal plateau of 1 hour 30 minutes at the end of heating, representing the residence time in the furnace. Upon removal from the furnace, the carbonized samples were cooled in a desiccator.

2.1.3. Purification

At the end of the production process, the cooled activated carbon is washed thoroughly with hot distilled water until the pH reaches between 6.5 and 7 to remove any impurities, then dried in an oven at 105°C for 24 hours. The processed activated carbon (PAC) is then cooled and stored in airtight containers until characterization tests are performed.

2.2.1. Yield calculation

The yield values for activated carbon production are determined using the following formula:

$$\text{Yield} = \frac{m_f}{m_i} \times 100 \qquad (1)$$

finalmass (m_f) and initial mass (m_i).

2.2.2. Surface function

The surface function is a characteristic that highlights the acidic and basic groups of CA. The method adopted for its determination is that of Boehm (1966), taken from the work of TCHAKALA et al [16], which is a return titration method. The basic groups are measured as a whole, while the acidic groups are measured separately. The experimental protocol is as follows: 0.2 g of CA was placed in contact with 20 mL of each of the aqueous solutions of NaOH, Na_2CO_3, $NaHCO_3$, C_2H_5ONa, and HCl at 0.1 M. Each solution was stirred for 24 hours to ensure that a maximum number of CA surface groups reacted, and then the mixture was filtered. After filtration, 10 mL of each of the five solutions was measured. The basic solutions were titrated with 0.1 M hydrochloric acid using three drops of bromothymol blue, phenolphthalein, bromocresol green, and helianthine, respectively, and the acidic solution was titrated with 0.1 M sodium hydroxide using bromothymol blue as the color indicator. As this is a back titration, the number of moles of the function sought corresponds to the number of moles that reacted with the contact solution. It is given by formula (2):

$$n_{éqR} = N_i V_i - N_f V_f \quad (2)$$

néqR is the number of equivalent grams that reacted; N_iV_i is the number of equivalent grams before the reaction; N_fV_f is the number of equivalent grams after the reaction.

2.2.3. pH at zero charge point (pH_{PCN})

Activated carbon in contact with a solvent has an acid-base character. However, there is a pH called pH at zero charge point (pH_{PCN}) at which it is electrically neutral in solution. To determine the (pH_{PCN}), the first bisector method was used. This method involves preparing 0.1 M sodium chloride (NaCl) solutions at pH values of 2, 4, 6, 8, and 10. The pH values were adjusted with a HI 991001 pH meter using NaOH and HCl solutions. 0.1 g of CA was placed in contact with 20 mL of each solution per sample. The mixture was stirred magnetically for 72 hours. The suspension was then filtered through filter paper and the pH of the filtrate was measured for each mixture. This allowed us to plot the curve pHi - pHf = f(pHi). The intersection point between this curve and the line x = 0 gives the pH at the zero loading point of the activated carbon in question.

2.2.4. Methylene blue (MB) index on synthesized activated carbons

The MB index, expressed in mg g^{-1}, represents the adsorption capacity of medium-sized molecules for the purpose of evaluating mesopores and macropores. MB adsorption was performed by introducing 0.1 g of CA, previously dried in an oven at 105°C, into a 250 mL Erlenmeyer flask containing 100 mL of the standard MB analysis solution. The mixture was stirred for 20 min. After this contact time, it was filtered through filter paper and the residual concentration of Methylene Blue in the solution was determined using a UV-visible spectrophotometer at a wavelength of 620 nm, which is the wavelength at which the adsorption of the MB molecule is maximum. Equation (3) gives the calculation of the Methylene Blue index.

$$Q_{BM} = \frac{(C_i - C_r)VM}{m} \times 100 \quad (3)$$

With Q_{BM}: adsorption capacity of C_A (in mg/g); C_i: initial concentration of BM solution (in mol/L); C_r: residual concentration of BM solution (in mol/L); V: volume of BM solution (in mL); M: molar mass of BM; m: mass of adsorbent used (in g)

2.3. Application for the treatment of chromium solution

Chromium removal from CA was carried out as follows: in a 100 mL beaker, a mass m of 50 mg of CA weighed using a precision balance (accurate to 1/10,000, Precisa brand) was added to 50 mL of Cr ($K_2Cr_2O_7$) solution of known concentration. The mixture was stirred for a specific period of time, then filtered through filter paper, and the residual Cr(VI) concentration was measured using a Micro-Plasma Atomic Emission Spectroscopy (MP-AES) flame spectrophotometer (Figure 1). The adsorption capacity and extraction yield of Cr are given by equations (4) and (5) respectively [10]:

$$q_{eq} = \frac{(C_i - C_f)V}{m_{CA}} \quad (4) \qquad et \quad R = \frac{(C_i - C_f)}{C_i} \times 100 \quad (5)$$

where qeq is the Cr adsorption capacity expressed in mg g^{-1}, Ci is the initial concentration of the Cr solution in mg L^{-1}, C_f is the final concentration of the Cr solution in mg L^{-1}, V is the volume of the Cr solution in mL, m_{CA} is the mass of activated carbon in g, and R is the Cr extraction yield in %.

Figure 1. Micro-Plasma Atomic Emission Spectroscopy MP-AES

2.3.1. Effect of contact time

2.3.1.1. Elovich kinetics

Equation (6) was used to study the Elovich kinetics of Cr-CAEs.

$$q_t = \frac{1}{\beta} ln(t) + \frac{1}{\beta} ln(\alpha\beta) \quad (6)$$

q_t is the amount of solute adsorbed at time t in mg g^{-1}, α is the initial adsorption rate in mg g^{-1} min^{-1}, and β is the Elovich constant in g.

The q_t curve as a function of time ln(t) is plotted. Thus, the characteristic indices of the Elovich model are determined from the slope = $\frac{1}{\beta}$ and the y-intercept = $\frac{1}{\beta}\ln(\alpha\beta)$ of the line.

2.3.1.2. External diffusion kinetics

Equation (7) was used to study the external diffusion kinetics of Cr-CAEs.

$$ln\left(\frac{C_0 - C_{eq}}{C_t - C_{eq}}\right) = k\left(\frac{a}{V}\right).t = k_{ed}.t \quad (7)$$

C_t is the concentration of Cr at time t expressed in mg L^{-1}, Ceq is the equilibrium concentration of Cr in mg L^{-1}, a is the area of the CAEs-Cr interface in cm^2, V is the volume of solution in mL, k_{ed} is the external diffusion constant, and t is the time in min.

The curve $\ln\left(\frac{C_0-C_e}{C_t-C_e}\right)$ as a function of time t is plotted. Thus, the characteristic indices of the model are determined.

2.3.2. Effect of CA mass

The variation in contact surface area (variation in CA mass) was carried out for a contact time of 2 hours. The masses considered were 20, 40, 60, and 80 mg of CA for 50 mL of chromium solution at 70 mg L^{-1}.

2.3.2. Effect of the pH of the dichromate solution

The pH of the chromium solution is an essential parameter for adsorption because there are four forms of chromium oxides depending on the pH and concentration. For this part, the contact time was set at 2 hours, the adsorbent mass at 80 mg, and the solution concentration at 70 mg/L. Thus, chromium removal was performed at pH = 2, 4, 6, 8, and 10.

2.3.3. Adsorption of chromium on Activated Carbon

3. Results and Discussion

3.1. Results

3.1.1. Mass yields of Activated Carbon

Figure 2 shows the results of the mass yields after pyrolysis for the 8 ACE samples.

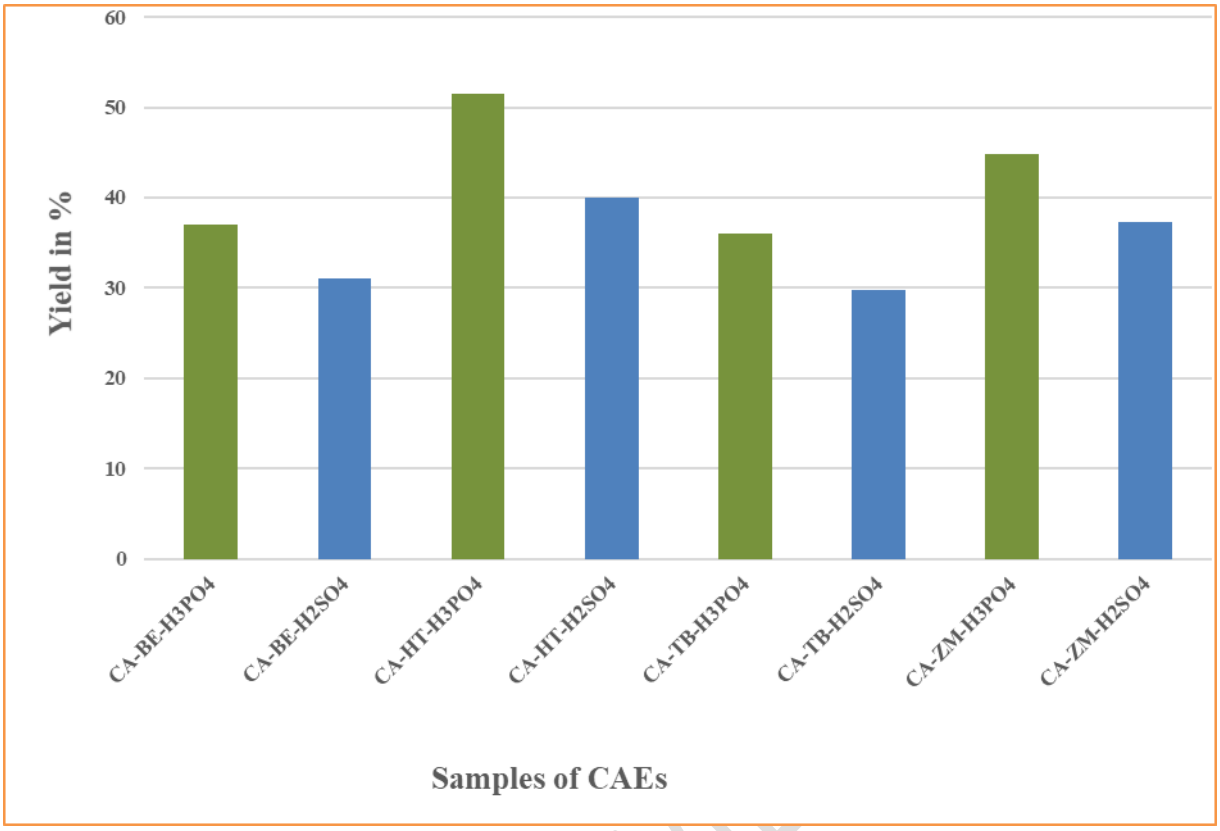

Figure 2. Mass yield after pyrolysis

3.1.2. Surface functions of activated carbons

The results of the surface functions of eight (8) ACEs and one AC-C in $m_{eq}\ g^{-1}$ are recorded in Table 1.

Table 1. Surface functions of CAEs and CA-C in $m_{eq}\ g^{-1}$

Elaborated activated carbons	Acids					Basics
	Carboxylic	Lactone	Phenol	Carbonyl	Totals	Globality
CA-BA-H_3PO_4	1.78	1.16	0.26	0,24	3.44	0
CA-BA-H_2SO_4	1.76	1.46	0.47	0,22	3.91	0
CA-HT-H_3PO_4	1.88	0.94	0.54	0,2	3.56	0
CA-HT-H_2SO_4	1.62	1.152	0.368	0,26	3.4	0
CA-TB-H_3PO_4	1.94	0.52	0.48	0,24	3.18	0
CA-TB-H_2SO_4	1.86	1.04	0.48	0,32	3.7	0
CA-ZM-H_3PO_4	1.8	1.16	0.34	0,16	3.46	0
CA-ZM-H_2SO_4	1.62	1.4	0.48	0,36	3.86	0
CA-C	0	2	0.1	1,2	3.3	0

The numbers of active CA sites are shown in Table 2.

Table 2. Number of active CA sites

Elaborated activated carbons	Acides x10^{23}					Basics Globality
	Carboxylic	Lactone	Phenol	Carbonyl	Totals	
CA-BA-H_3PO_4	10.71	6.98	1.56	1.44	20.71	-
CA-BA-H_2SO_4	10.59	8.79	2.83	1.32	23.54	-
CA-HT-H_3PO_4	11.32	5.66	3.25	1.20	21.43	-
CA-HT-H_2SO_4	9.75	6.93	2.21	1.56	20.47	-
CA-TB-H_3PO_4	11.68	3.13	2.89	1.44	19.14	-
CA-TB-H_2SO_4	11.20	6.26	2.89	1.92	22.28	-
CA-ZM-H_3PO_4	10.83	6.98	2.04	0.96	20.83	-
CA-ZM-H_2SO_4	9.75	8.43	2.89	2.16	23.24	-
CA-C	0	12.04	0.60	7.22	19.87	-

3.1.3. pH at zero charge point of CAEs and CA-C

The pH_{PCN} or pH at zero charge point corresponds to the pH value at which the net charge on the CA surface is zero, even though positive and negative charges are still present. Figure 3 shows the pH_{PCN} results for CAEs.

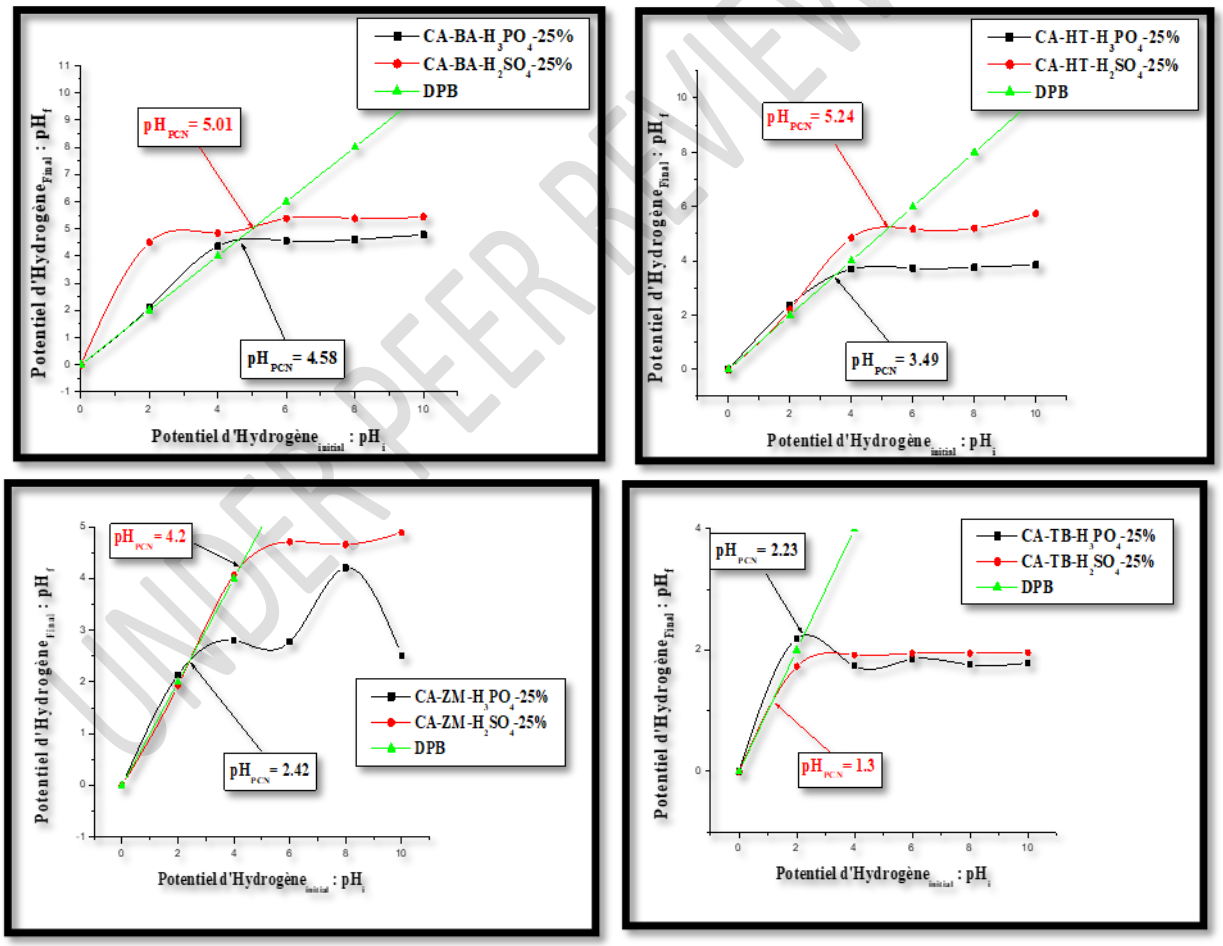

Figure 3.pH_{PCN} of CAEs in H_3PO_4 and H_2SO_4

3.1.4. Methylene Blue Index

Figure 4 shows the MB extraction rates for the 8 CAE samples and the CA-C sample.

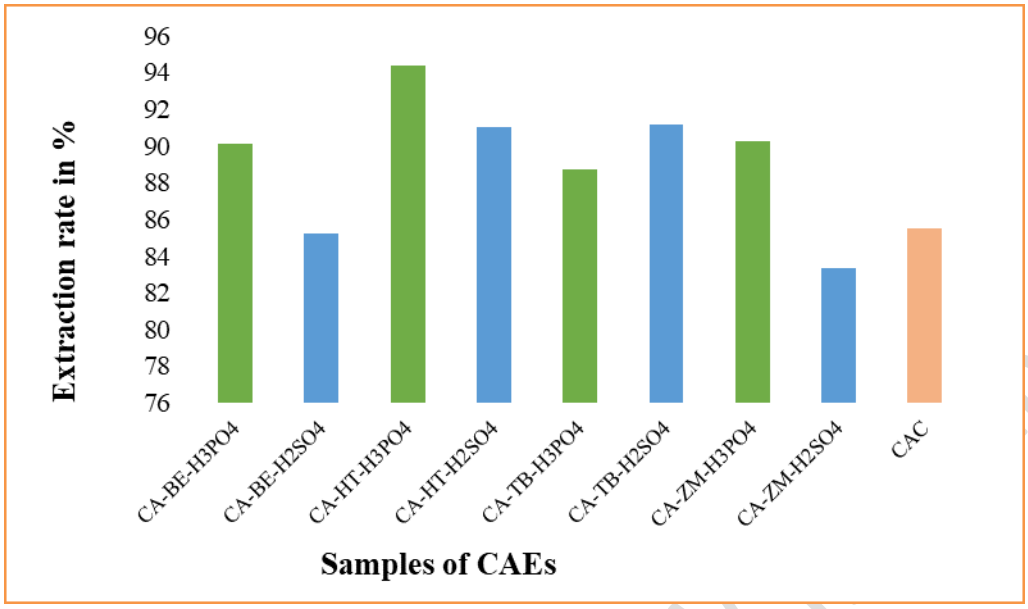

Figure 4: CAE BM Index and CA-C

Figure 5 shows the results of applying linearization of the Elovich model based on experimental data.

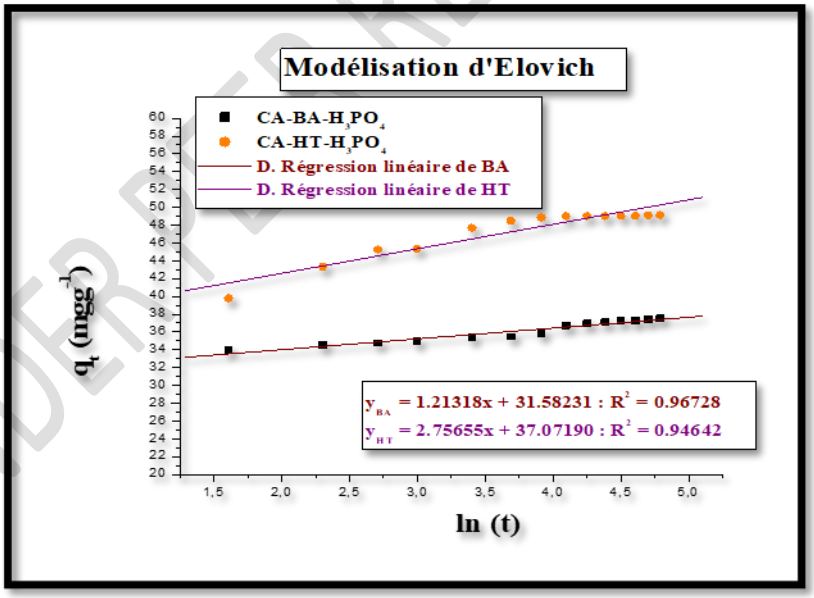

Figure 5: Elovich kinetics

The characteristic parameters of Elovich kinetics are summarized in Table 3.

202 Table 3. Parameters of Elovich kinetics

Parameters	A (mg g^{-1} min^{-1})	β (g mg^{-1})	αβ (min^{-1})	R^2
CA-BA-H_3PO_4	$2.45343.10^{11}$	0.82427	$2.02228.10^{11}$	0.96728
CA-HT-H_3PO_4	$1.91005.10^{6}$	0.36277	$6.92908.10^{6}$	0.94642

203 **3.1.3. External diffusion kinetics**

204 Figure 6 shows the results of applying linearization of the external diffusion model based on
205 experimental data from CAEs.

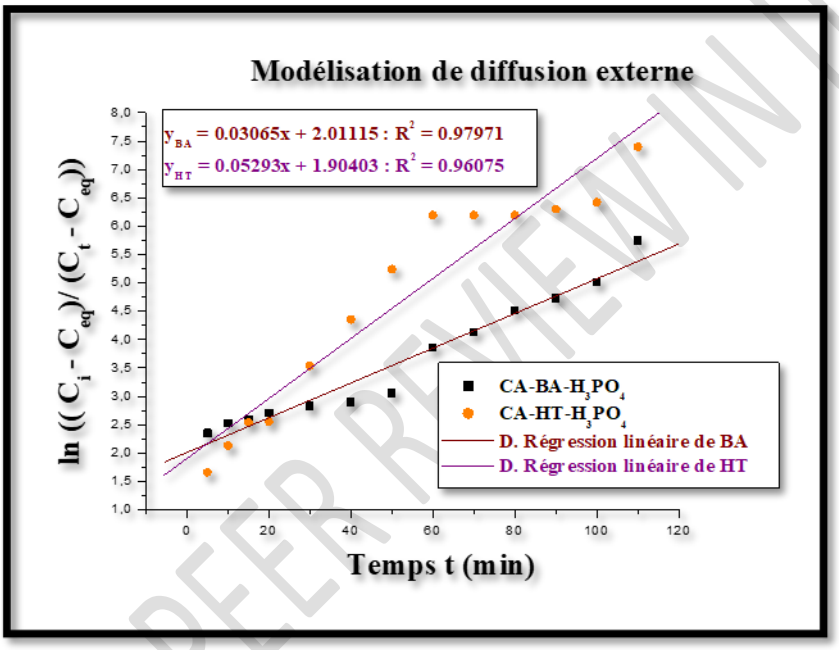

206

207 Figure 6. External diffusion kinetics

208 The characteristic parameters of external diffusion kinetics are summarized in Table 4.

209 Table 4: External diffusion parameters

Parameters	D (cm^2 min^{-1})	k_d min^{-1}	R^2
CA-BA-H_3PO_4	0.07643	0.01312	0.97898
CA-HT-H_3PO_4	0.13219	0.02269	0.96157

210 **3.1.4. Intra-particle diffusion kinetics**

211 Figure 7 shows the curves resulting from the application of the intra-particle diffusion model
212 based on experimental data from CAEs.

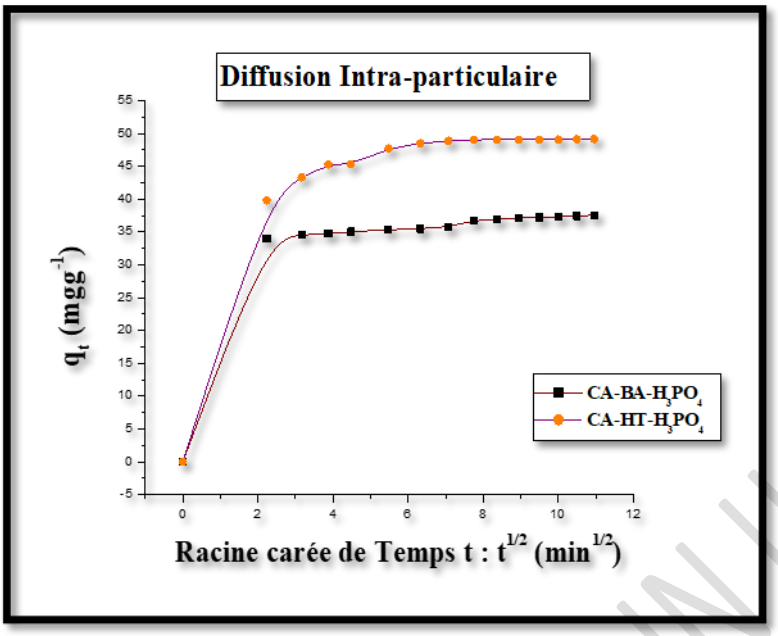

Figure 7. Intra-particle diffusion kinetics

3.1.5. Mass effect of CAEs

Figure 8 shows the Cr removal rate as a function of CAE mass (CA-BA-H_3PO_4 and CA-HT-H_3PO_4).

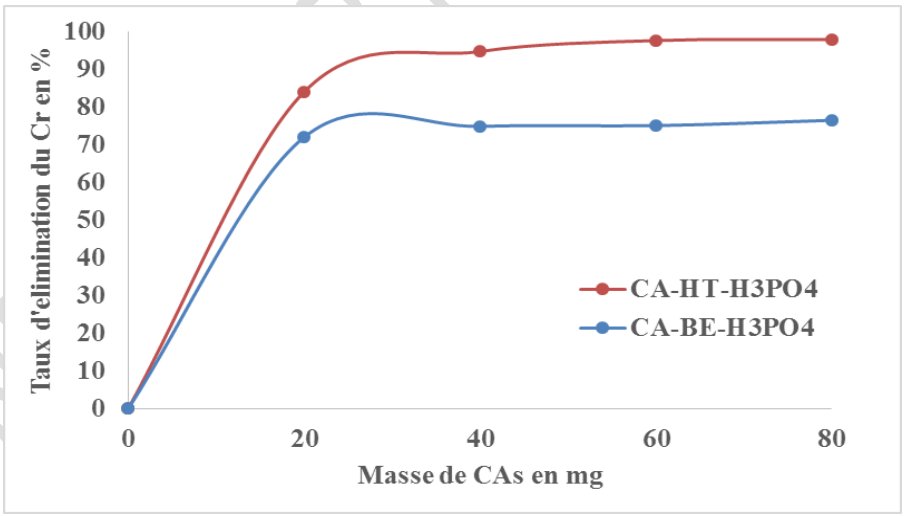

Figure 8. Mass effect of CAEs

3.1.6. Effect of solution pH

Figure 9 shows the Cr removal rate as a function of the pH of the chromium solution for CAEs (CA-BA-H_3PO_4 and CA-HT-H_3PO_4).

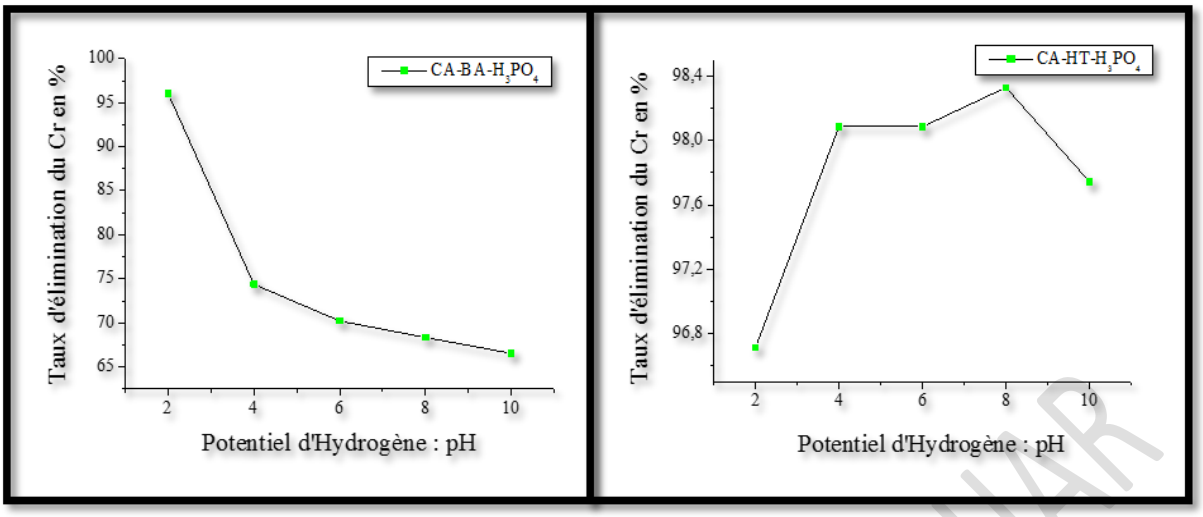

Figure 9. Effect of Cr solution pH on PACs

3.1.7. Chromium adsorption on processed activated carbon

Figure 10 shows the chromium removal rate on PACs at 25% and PAC under the optimal operating conditions obtained.

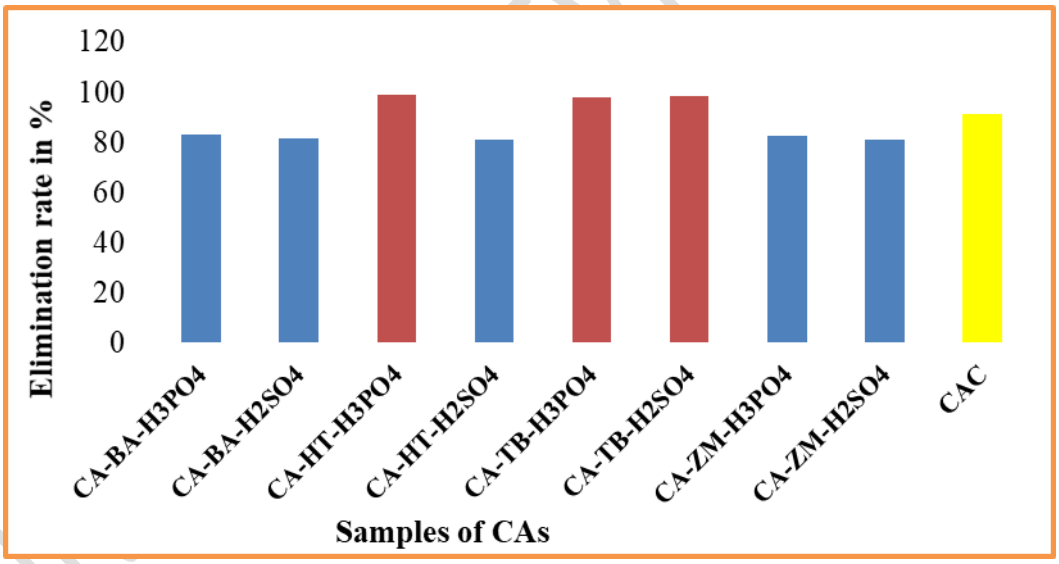

Figure 10. Adsorption of chromium on CAs

3.2. Discussion

The mass yield results presented in Figure 2 show that these yields vary from 29.8 to 51.55% for TB and HT, respectively. In both activation cases, the best yields are obtained with HT: 51.55% (H_3PO_4) and 40% (H_2SO_4). This is consistent with the results of thermal analyses performed on BA and HT nut shells. Regardless of the biomass, the best yields are obtained

by activation with H_3PO_4. This would confirm the fact that H_3PO_4 acid delays the thermal decomposition of biomass and limits the loss of volatile matter, leading to the formation of a rigid carbon matrix, i.e., AC [17]. Although the CA production process used is very simple, the mass yield from HT is greater than 50%. This is comparable to commercial activated carbons [10].

Analysis of these results, presented in Table 2, shows a complete absence of basic function. This can be explained by the fact that the CAEs were not exposed to oxygen below 200°C or above 700°C, they were not treated with hydrogen, and they were not degassed at room temperature, as this is the stage at which basic functions are introduced. This would indicate that CA-C did not undergo this treatment either. In addition, CAC did not develop carboxyl functions. The surface functions are acidic in nature, and the total acidity of the ACEs increased from 3.18 to 3.91 m_{eq} g^{-1} for CA-TB-H_3PO_4 and CA-BA-H_3PO_4, respectively. These results suggest that the samples have a high degree of adsorption. The literature shows that the higher the functional group content, the greater the degree of adsorption of activated carbon [18,19]. Similar results have been reported by several authors, such as Daoud and Benturki in 2014 [20], Reffas et *al*., in 2010 [21], Souley in 2015 [22], and Siragi et *al*., in 2017 [11].

The results presented in Figure 3 show that the pH values at zero loading point for CAEs and commercial activated carbon are all below neutrality (pH < 7). They range from 1.3 to 5.24 for the activated carbons developed. Commercial activated carbon gave a value of 6.84 (Appendix). These results are consistent with the surface function results found. Similar results were reported by Siragi et *al*., in 2017 [11]. In fact, the values obtained for the developed activated carbons are significantly different from those found by Rabilou (2015) [22,23]. This can be explained by the washing method used after development. For commercial activated carbon, the value found is not significantly different (6.9).

The results presented in Figure 4 show that BM extraction rates vary from 83.3445 to 94.3777%. In general, activated carbons produced by H_3PO_4 acid activation develop better BM extraction rates regardless of the biomass used. In fact, under the operating conditions, six (6) CAE samples developed BM extraction rates higher than that obtained with CA-C. The CA that developed the highest BM extraction rate was obtained with HT.

The results of Elovich kinetic modeling presented in Figure 5 and Table III show that the correlation coefficient values (R^2) are approximately 0.96728 and 0.94642 for CA-BA-H_3PO_4 and CA-HT-H_3PO_4, respectively. This shows that CA-BA-H_3PO_4 is better suited to this model than CA-HT-H_3PO_4. The initial Cr adsorption rate α calculated with CA-BA-H_3PO_4 (2.45343.1011 mg g^{-1} min^{-1}) is greater than that obtained with CA-HT-H_3PO_4 (1.91005.106 mg g^{-1} min^{-1}). The same is true for the calculated constant values (related to the external surface area and activation energy of chemisorption), which are approximately 0.82427 and 0.36277 g mg^{-1} for CA-BA-H_3PO_4 and CA-HT-H_3PO_4, respectively, and the same for the αβ product. Analysis of these different parameters shows that the Elovich model could describe the experimental data. Indeed, there is a similarity between the latter and the assumption made by Chien and Clayton [24] that $\alpha\beta t \gg 1$ based on the model data. It should be noted that this model could confirm the existence of activated chemisorption according to Feng et al. [25], which could explain the second steps observed on the kinetic curves, but it does not provide any precise mechanism of interaction between CAEs and Cr.

The results of external diffusion modeling show that the correlation coefficient values (R^2) are approximately 0.97898 and 0.96157 for CA-BA-H_3PO_4 and CA-HT-H_3PO_4, respectively. This shows that CA-BA-H_3PO_4 is better suited to this model than CA-HT-H_3PO_4. However, the mass diffusivity D calculated with CA-BA-H_3PO_4 (0.07643 cm^2 min^{-1}) is lower than that obtained with CA-HT-H_3PO_4 (0.13219 cm^2 min^{-1}). Thus, the values of the constants related to this model follow the same logic and are of the order of 0.01312 and 0.02269 min^{-1} for CA-BA-H_3PO_4 and CA-HT-H_3PO_4, respectively. This shows that despite the higher correlation coefficient of CA-BA-H_3PO_4, the mass diffusion coefficient is higher for CA-HT-H_3PO_4.

According to Figure 7, all of the curves plot show multi-linearities suggesting the existence of several stages in the Cr sorption process. These multi-linearities revealed by this model indicate the presence of three stages involved in the Cr adsorption process. The first stage, which is slightly concave and faster, can be considered as the binding of Cr to active sites on the outer surface of CAEs (instantaneous adsorption), and the second, slower stage can be attributed to the diffusion of Cr inside the pores of CAEs (gradual adsorption). The third stage is a plateau corresponding to equilibrium. The curves are not straight lines passing through the origin, which shows that internal diffusion is not the only factor limiting the kinetics of Cr sorption on CAEs. Other mechanisms may therefore be involved in this case [26,27].

The results obtained show that increasing the contact surface area of CAEs increases the percentage of Cr extraction.

Figure 9 shows that the optimal adsorption pH values for chromium are 2 and 8 for CA-BA-H_3PO_4 and CA-HT-H_3PO_4, respectively. According to the Mohan and Pittman diagram, the best-adsorbed chromium species is $HCrO_4^-$ for CA-BA-H_3PO_4 and CrO_4^{2-} for CA-HT-H_3PO_4.

Analysis of Figure 10 shows that the extraction rate increases from 80.82% to 98.98%. It should be noted that the yields of our three CAE samples exceed that of CAC (91.48%).

4. Conclusion

At the end of this study, the following lessons were learned:

- ✓ The best yields are obtained with HT; 51.55% (H_3PO_4) and 40% (H_2SO_4) ;
- ✓ Regardless of the biomass, the best yields are obtained by activation with H_3PO_4;
- ✓ the total absence of basic functions. The surface functions are acidic in nature and the total acidity of the CAEs would increase from 3.18 to 3.91 meq g^{-1} for CA-TB-H_3PO_4 and CA-BA-H_3PO_4respectively;
- ✓ The pH values at zero loading point for CAEs and commercial products are all below neutrality (pH < 7). They range from 1.3 to 5.24 for activated carbons;
- ✓ BM extraction rates range from 83.3445 to 94.3777%;
- ✓ The correlation coefficient values (R^2) are approximately 0.96728 and 0.94642 for CA-BA-H_3PO_4 and CA-HT-H_3PO_4, respectively.
- ✓ The initial Cr adsorption rate "α" calculated with CA-BA-H_3PO_4 (2.45343.1011 mg g^{-1} min^{-1}) is greater than that obtained with CA-HT-H_3PO_4 (1.91005.106 mg g^{-1} min^{-1});
- ✓ the mass diffusivity D calculated with CA-BA-H_3PO_4 (0.07643 cm^2 min^{-1}) is lower than that obtained with CA-HT-H_3PO_4 (0.13219 cm^2 min^{-1});
- ✓ The results obtained show that increasing the contact surface area of CAEs increases the percentage of Cr extraction;
- ✓ The optimal adsorption pH values for chromium are 2 and 8 for CA-BA-H_3PO_4 and CA-HT-H_3PO_4, respectively. It should be noted that the yields of the three CAE samples exceed that of CAC (91.48%).

References:

[1]. Ayral, C. (2009). Elimination de polluants aromatiques par oxydation catalytique sur charbon actif. Thèse de doctorat à l'Institut National Polytechnique de Toulouse à l'Université de Toulouse, Toulouse-France TF, 186.

[2]. Gueye, M. (2015). Développement de charbon actif à partir de biomasse lignocellulosique pour des applications dans le traitement de l'eau. Thèse de doctorat à l'Institut International de l'Eau et de l'Environnement (2iE), Ouagadougou/ Burkina Faso OBF, 215.

[3]. Ousmaila, SM. Valorization of agro-food wastes for the elaboration of activated carbons; characterization and application in the depollution of wastewater loaded with chromium from the Malam Yaro Tannery of Zinder-Niger. [Doctoral thesis]. Abdou Moumouni University of Niamey. These of Doctorate Chemistry of Metals ; 2019.

[4]. Ousmaila S.M, Maˆazou S.D.B, Mousbahou M.A.M, Ibrahim N. Valorisation des coques de noyaux de Balanites aegyptiaca (L.) Del. et Hyphaene th´ebaica (L.) Mart, pour l'´elaboration et caracterisation de Charbons Actifs; application pour l'elimination du chrome. ESJ 14 (2018) 195, https://doi.org/10.19044/esj.2018.v14n21p195

[5]. Krishnamoorthy, G., Sadulla, S., & Sehgal1, P.K. (2012). Asit Baran Mandal, Green chemistry approaches to leather tanning process for making chrome-free leather by unnatural amino acids : Journal of Hazardous Materials, **Vol. 215–216**, 173–182. DOI :https://doi.org/10.1016/j.jhazmat.2012.02.046

[6]. Combéré, W., Arsène, H. Y., Abdoulaye, D., & Kaboré, L. (2017). Elimination du chrome trivalent des eaux par des zéolithes échangées au fer et des argiles naturelles du burkina faso : J. Soc. Ouest-Afr. Chim. **043**, 26- 30.

[7]. Siragi D. B M, Desmecht D, Hima H. I, Mamane O. S, Natatou I. Optimization of Activated Carbons Prepared from Parinari macrophylla Shells. MSA, vol.12, no 05, 2021, p. 207-222, doi: 10.4236/msa.2021.125014.

[8]. Ousmaila, S. M., Maâzou, S.B.D., Abdoul Rachid, C. Y.,Maman Mousbahou, M. A. &Ibrahim N. (2018). Valorisation de coques de noix de *Balanites aegyptiaca* (L.) Del.et élimination du chrome en solution :Afrique SCIENCE, **14** (3) 167 – 181.

[9]. Ait, S. F. (2011). Adsorption du phénol par un mélange d'adsorbants (bentonite - charbon actif).Magister à l'Université de Boumerdèz UB, Boumerdèz-Algerie BA, 106.

[10]. Ousmaila, S.M., Adamou, Z., Ibrahim, D., & Ibrahim, N. (2016). Préparation et caractérisation de charbons actifs à base de coques de noyaux de Balanites eagyptiaca et de Zizyphus mauritiana : J. Soc. Ouest-Afr. Chim. 041, 59- 67.

[11]. Maâzou, S.D.B., Hima, I. H., Maman Mousbahou, M. A., Adamou, Z., & Ibrahim, N. (2017). Elimination du chrome par du charbon actif élaboré et caractérisé à partir de la coque du noyau de Balanites agyptiaca : Int. J. Biol. Chem. Sci. 11 (6) 3050-3065. DOI : https://dx.doi.org/10.4314/ijbcs.v11i6.39.

[12]. Zeroual, S., Guerfi, K., Hazourli, S. & Charnay, C. (2011). Estimation de l'hétérogénéité d'un charbon actif oxydé à différentes températures à partir de l'adsorption des molécules sondent : Energies Renouvelables, **14** (4) 581-590.

[13]. Avom, J., Mbadcam, J. K., Matip, M. R. L., Germain, P. (2001). Adsorption isotherme de l'acide acétique par charbons d'origine végétale : AJST, Science and Engineering séries, **2** (2) 1-7. DOI : http://dx.doi.org/10.4314/ajst.v2i2.44663

[14]. Kheliel, O. (2014). Etude du pouvoir adsorbant du charbon actif pour la dénitrification des eaux souterraines. Mémoire de Master à l'Université Mohamed Khider Biskra UMKB, Alger-Algérie AA.

[15]. Mahamane Nassirou Amadou Kiari, Affou Tindo Sylvie Konan, Ousmaila Sanda Mamane, Leygnima Yaya Ouattara, Maman Hamissou Ibrahim Grema,Maˆazou Siragi Dounounou Boukari, Abdourahamane Adamou Ibro, Maman Mousbahou Malam Alma, Kouassi Benjamin Yao. Adsorption kinetics, thermodynamics, modeling and optimization of bisphenol A on activated carbon based on Hyphaene Thebaica shells. 2666-0164/© 2024 The Authors. Published by Elsevier Ltd. This is an open access article under the CC BY-NC-ND licenseN(http://creativecommons.org/licenses/bync-nd/4.0/). pp. 01 à 13 , 2024

[16]. Tchakala, I., Bawa, L. M., Djaneye-Boundjou, G., Doni, K.S., & Nambo, P. (2012). Optimisation du procédé de préparation des charbons actifs par voie chimique (H_3PO_4) à partir des tourteaux de Karité et des tourteaux de Coton : Int. J. Biol. Chem. Sci. **6** (1), 461–478. DOI :http://dx.doi.org/10.4314/ijbcs.v6i1.42

[17]. Zhao, J., Lai, C., Dai, Y. & Xie, J. (2007). Pore structure control of mesoporous carbon as supercapacitor material : Materials Letters., **61**, 4639-4642. DOI : https://doi.org/10.1016/j.matlet.2007.02.071

[18]. Gueye, M., Richardson, Y., Kafack, F.T. & Blin, J. (2014). High efficiency activated carbons from african biomass residues for the removal of chromium (VI) from wastewater :

Journal of environmental chemical engineering**2** (1), 273-281. DOI :http://doi.org/101007/s10450-017-9929-7 .

[19]. Cronje, K.J., Chetty, K., Carsky, M., Sahu, J.N., & Meikap, B.C. (2011). Optimization of chromium (VI) sorption potential using developed activated carbon from sugarcane bagasse with chemical activation by zinc chloride. Journal Desalination **275,** 276-284.

[20]. Daoud, M. & Benturki, O. (2014). Activation d'un charbon à base de noyaux de jujubes et l'application à l'environnement : Revue des Energies Renouvelables, SIENR'**14** Ghardaïa 155-162.

[21]. Reffas, A., Bernardet, V., David, B., Reinert, L., Bencheikh, M., Lehocine, Dubois, M., Batisse, M. N. & Duclaux, L. (2010).Carbons prepared from coffee grounds by H_3PO_4activation: Characterization and adsorption of methylene blue and Nylosan Red N-2RBL : Journal of Hazardous Materials **175** (1-2) 779-788 DOI : https://doi.org/10.1016/j.jhazmat.2009.10.076

[22]. Souley, M. R. (2015). Elaboration du charbon actif en poudre à partir de la coque de Balanites aegyptiaca et de la coque de Zizyphys mauritiaca : Mémoire de master à l'Université Abdou Moumouni UAM, Niamey-Niamey NN, 69.

[23]. Rabilou Souley Moussa, Ousmaila Sanda Mamane, Issa Habou, Maman Mousbahou Malam Alma and Ibrahim Natatou.Determination of the surfaces functions and of the pH at the point of zero charges of powdered activated carbons produced from the shells of the nucleus of Balanites aegyptiaca and Zizyphus mauritiana.World Journal of Advanced Research and Reviews Article DOI:https://doi.org/10.30574/wjarr.2022.16.3.143. pp. 893 à904 . 2022

[24]. Chien S. H. & Clayton W. R. (1979). Application of Elovich equation to the kinetics of phosphate release and sorption in soils : Soil Sci. Society America J., **44** (2) 265 – 268. DOI : https://doi:10.2136/sssaj1980.03615995004400020013x

[25]. Feng-Chin W., Ru-Ling T. &Ruey-Shin J. (2009). Characteristics of Elovich equation used for the analysis of adsorption kinetics in dye-chitosan systems. Chem. Eng. J., **150**,366-373. DOI : https://doi.org/10.1016/j.cej.2009.01.014

[26]. Sarkara M., Acharya P.M. & Bhattacharya B. (2003). Modeling the adsorption kinetics of some priority organic pollutants in water from diffusion and activation energy parameters. J. Coll. Int. Sci**.,266** (1) 28 – 32. DOI : https://doi.org/10.1016/S0021-9797(03)00551-4

[27]. Srivastava V. C., Swamy M. M., Malli D., Prasad B. & Mishra I. M. (2006) Adsorptive removal of phenol by Bagasse fly ash and activated carbon: Equilibrium, Kinetics

and Thermodynamics. Coll. Surf. A: Physicochemical and Engineering Aspects, **272** (1-2) 89 – 104. DOI : https://doi.org/10.1016/j.colsurfa.2005.07.016